PHYSICAL REVIEW E VOLUME 52, NUMBER 4 OCTOBER 1995

Phase diagrams of nearly hard-sphere binary colloids

A. D. Dinsmore and A. G. Yodh
Department of Physics, University of Pennsylvania, Philadelphia, Pennsylvania 19104

D. J. Pine
Exxon Research and Engineering Company, 79 Route 22 East, Annandale, New Jersey 08801

(Received 16 March 1995; revised manuscript received 9 June 1995)

We have investigated the equilibrium compositions and structures of the phases of nearly-hard-sphere binary colloids and obtained experimental phase diagrams. Aqueous dispersions of charge-stabilized polystyrene spheres were studied in the hard-sphere limit, with sphere-diameter ratios ranging from 2 to 12 and total volume fractions less than 0.4. At sufficiently high volume fractions, the samples separated into two phases. One phase, consisting primarily of small spheres, is a disordered fluid. In the other phase, the large spheres form an ordered crystalline solid which is permeated by a disordered fluid of small spheres. Previously reported crystallites on the surface of the sample cell were demonstrated to have the same structure as the bulk crystals and are assumed to be a wetting of the bulk phase. A simple model of the bulk phases is described and free energies calculated. The predicted phase diagrams agree closely with the results of computer simulations and with our experimental results.

PACS number(s): 82.70.Dd, 64.70.−p, 64.60.Cn, 65.50.+m

I. INTRODUCTION

Colloidal dispersions have attracted considerable attention as a result of their rich thermodynamic properties [1] and their industrial and medical utility. For example, in materials such as paint, ink, plaster, cosmetics, food, and blood, an understanding of particle dynamics and aggregation is of tremendous practical importance.

A thorough understanding of the hard-sphere system is important because calculations for nonideal systems often begin with the hard-sphere model. We are interested in mixtures of hard spheres of two different sizes. These binary mixtures exhibit a very rich phase behavior which depends on three dimensionless parameters: the volume fractions ϕ_L and ϕ_S of the large and small spheres, respectively, and the ratio, α ($\equiv a_L/a_S$), of the large- and small-sphere diameters, a_L and a_S. The thermodynamic behavior of hard-sphere systems is independent of temperature. We have performed experiments on charge-stabilized polystyrene spheres dispersed in water. Because the interparticle repulsion is screened to a very short range (less than 1% of a_L), these particles closely resemble hard spheres. Using optical microscopy, diffusing-wave spectroscopy [2], and Kossel scattering [3], we have probed the structures and compositions of the samples *in situ.* We have also used scanning electron microscopy to study dried samples.

In this paper, we describe systematic measurements of the volume fractions (ϕ_L and ϕ_S) of the bulk and surface phases at equilibrium and we present experimental phase diagrams. In the bulk of the sample, we observed coexisting fluid and solid phases. Two-fluid coexistence was not observed, even in samples with α as low as 2.0. Typically, the solid phase is a random stacking of close-packed planes of large spheres, permeated by a dilute fluid of small spheres. The surface crystals [4] were determined to have the same structure as the bulk solid.

A calculation of the phase diagram for binary hard-sphere mixtures is also presented. In particular, we propose a simple model for the fluid phase which accounts for the hard-sphere nature of all of the particles. For the solid phase, we use geometric arguments to calculate the free energy of the large-sphere crystal [5] and the free energy of the small-sphere fluid which permeates the crystal. Our approach predicts phase separation in *monodisperse* hard-sphere colloids with coexisting fluid and solid volume fractions 0.50 and 0.57, in reasonable agreement with the results of computer simulations (0.49 and 0.55, respectively) [6] and experiments [7]. For the *binary*-colloid case, our approach predicts fluid-solid phase separation at much lower total volume fractions than in monodisperse colloids, in agreement with our measurements. Our results and assumptions are discussed and compared to those of Lekkerkerker and co-workers [8,9] and of Poon and Warren [10], who consider binary hard-sphere colloids and colloid-polymer mixtures.

Hard-sphere systems lack the attractive interactions which typically compete with the tendency toward disorder (increased entropy). Nonetheless, as Asakura and Oosawa [11] have noted, an ordered arrangement of the large spheres can *increase* the total entropy of the system by increasing the entropy of the small spheres. Because the center of mass of a small sphere cannot penetrate within $a_S/2$ of a large sphere's surface (Fig. 1), a region of "excluded volume" surrounds each large sphere. When the surfaces of two large spheres approach within a small-sphere diameter, these excluded-volume regions overlap one another, so that the volume accessible to the center of mass of the small spheres increases. Thus the *entropy* of the small spheres increases, resulting in an attractive

1063-651X/95/52(4)/4045(13)/$06.00

"depletion" force between large spheres. When the small spheres sufficiently outnumber the large ones, a simple model shows that the energy of the depletion attraction is approximately $-1.5\alpha\phi_S k_B T$ [12], which can be a few $k_B T$ in magnitude. The energy of attraction between a large sphere and a flat, hard wall is approximately twice as great [4].

In the first attempt to calculate a phase diagram for binary hard-sphere mixtures, Lebowitz and Rowlinson [13] applied the Percus-Yevick approximation for binary hard-sphere fluids and predicted *no* phase separation for any α, ϕ_L, or ϕ_S. More recent attempts using density functional theory [14,15] have predicted a spinodal instability in systems with $\alpha > 5$. These approaches, however, have not determined the structures or compositions of the coexisting phases. A more phenomenological approach has also been used, in which one first assumes the structures of the coexisting phases, then computes the free energy and minimizes it to determine the phase diagram. Recently, Poon and Warren [10] (discussed in further detail in Sec. IV) calculated a phase diagram for mixtures with $\alpha = 7.1$. In this approach, the melting and freezing volume fractions of a monodisperse mixture must be assumed. Furthermore, the free energy of the large-sphere crystal is obtained from computer simulations, so that the underlying physics is somewhat obscured. Our model predicts the freezing and melting points of monodisperse mixtures. We also discuss a first-principles derivation of the Helmholtz free energy of the large-sphere crystal based on simple geometric considerations [5].

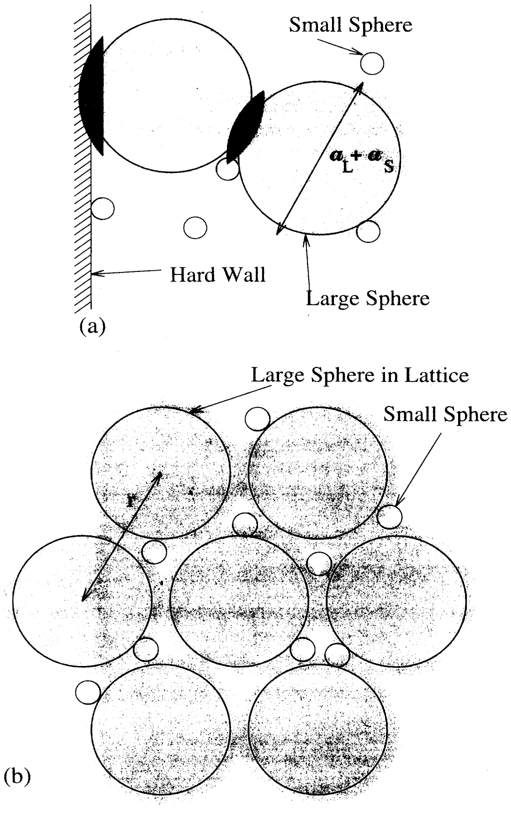

FIG. 1. Drawing of large and small spheres showing the excluded-volume regions described in the text. (a) The small-sphere centers of mass cannot penetrate within the shaded regions. When the large spheres approach one another or the wall, these excluded-volume regions overlap, increasing the volume accessible to the small spheres by the volume of the heavily shaded regions. (b) Diagram of the solid phase. The white regions represent the volume accessible to the small spheres, defined in Sec. IV as $(\xi + \gamma)V$.

In concentrated mixtures of similar-sized hard spheres (α approximately 1.7, total ϕ approximately 0.5), a variety of crystal structures, such as AB_{13} and AB_2, have been observed [16]. Relative thermodynamic stabilities of various solid-phase structures as a function of α have been calculated [17] and phase diagrams derived for hard-sphere mixtures with $\alpha = 1.2$ and 1.5 [18]. In general, phase separation in mixtures with such low α occurs only when the total volume fraction exceeds approximately 0.5, at which concentration the structure is largely determined by packing geometry and is thus strongly α dependent. The phases observed in this size-ratio regime are quite different from those observed in mixtures with $\alpha \geq 6$. Experiments in this latter regime have been done using silica spheres [19] and polystyrene spheres [4,20] in the hard-sphere limit. *These experiments, however, left undetermined the structures and compositions of the bulk phases at equilibrium.* Our experiments are the first to address the question of the structure of the dense phase in equilibrium.

Phase separation induced by the depletion force has been observed in monodisperse colloids with added polymer [21–23], in monodisperse emulsions with added polymer [24], and in binary emulsions [25]. In theoretical models, Gast and Russel [26] and Lekkerkerker and coworkers [8,9] assume that the small (polymer) particles are an ideal gas. This approximation is not very accurate for the mixtures of hard spheres we consider here. While there are similar features, polymers and emulsions are in general neither hard nor spherical, so the thermodynamics are somewhat different from the hard-sphere systems considered in this paper, as discussed below.

II. EXPERIMENTAL TECHNIQUE

A. Sample preparation

Our samples consist of submicrometer charge-stabilized polystyrene spheres dispersed in water. The small-sphere diameter (a_S) is 0.069 μm, and the large-sphere diameter (a_L) ranges from 0.137 to 0.825 μm. The particles' index of refraction is 1.58, large enough so that a 1-mm-thick sample of the large spheres multiply scatters visible light. We purchased stock solutions from a manufacturer (Seradyn, Indianapolis, IN, USA) in bottles containing particles of one size with less than 2% variation of diameters.

The polystyrene microspheres are not perfect hard spheres. Their interaction is described by the Derjaguin-Landau-Vermeer-Overbeek (DLVO) theory [27]. At very close range, there is a strong attraction due to the van der Waals force. A slightly longer-range Coulombic repulsion, due to charged sulfate groups on the sphere surfaces, acts as a barrier to the Van der Waals attraction, thus preventing irreversible aggregation of the particles. Seradyn manufactures solutions with enough salt dissolved in the water (approximately $0.01M$) to screen the Coulombic repulsion to short distances. As reported in Ref. [4], measurements of the lowest volume fraction at which 0.205-μm spheres crystallize indicate that the effective particle radius exceeds the physical radius by less than 4 nm. Thus we used the stock solutions as delivered. We found that purifying the particle solutions and adding more salt do not affect the results. Bulk and surface [4] crystals could be melted by shaking or by addition of enough filtered water to reduce the volume fractions below the liquidus curve. Thus the spheres in the solid phase were not held together by the irreversible van der Waals attraction. Furthermore, after storing five samples with the same ϕ_S and ϕ_L at different temperatures (5 °C, 20 °C, and 55 °C), we observed no deviation of the liquidus curve with changing temperature. Since the equilibrium state of hard-sphere systems is independent of temperature, we interpreted this result as further evidence of the nearly ideal hard-sphere nature of the polystyrene particles.

The mass density of the polystyrene particles is 5.0% greater than that of the surrounding water. While Brownian motion maintains single particles with diameters as large as 0.8 μm in suspension for several days, particle clusters settle to the bottom within a few hours. Therefore, in our samples, the bulk solid phase fell to the bottom of the sample and the fluid phase rose to the top, making it possible to identify phase separation by eye. All behaviors reported in this paper were observed within two days, often within 12 h. Several samples were prepared with enough heavy water to make the polystyrene neutrally buoyant. As discussed below, we found that gravitational sedimentation had a negligible effect on the equilibrium structure.

B. Measurement techniques

We determined the volume fractions of the stock solutions by weighing samples before and after drying in an oven. Solutions of spheres of two different sizes were mixed in glass, quartz, or polystyrene cuvettes 1–10 mm in thickness, 10 mm in width, and approximately 0.3–1.0 ml in volume. The initial volume fractions ϕ_S and ϕ_L were measured to a precision of approximately 1% by weighing the ingredients as they were added. Immediately after mixing, we thoroughly shook the samples by hand and in an ultrasonic bath. They were then stored at room temperature in a vertical position. For most ϕ_S and ϕ_L investigated, multiple samples were mixed, giving consistent results.

We directly observed the structure of the binary colloids in equilibrium using an optical microscope. After mixing, some samples were injected into cells approximately 100 μm thick, made of glass slides, standard cover slips, and 5-min epoxy. Using the optical microscope (Zeiss Axiovert 135), we could observe individual large spheres as they formed clusters. After approximately two days, when no further phase separation was observed, we determined the structure of the crystalline phase by direct observation. To verify that crystallization was not affected by the small volume of the cell, we let samples phase separate in 1-mm-thick cuvettes, extracted the sediment with a syringe, and injected it into a thin cell for viewing under the optical microscope. No differences between thin-cell and thick-cell samples were observed.

To measure ϕ_L and ϕ_S in the equilibrium bulk fluid phase, we carefully extracted the fluid from the top of two-day old samples using a syringe. Some of this supernatant was weighed, dried in an oven for two days, and weighed again to measure to within 1% the total volume fraction in the fluid phase, $\phi_L^{fl} + \phi_S^{fl}$, where the superscript fl denotes the fluid phase at equilibrium. The rest of the supernatant was diluted with a measured amount of filtered water so that the average distance between large spheres was much greater than the particle diameter (for imaging clarity). The small spheres, 0.069 μm in diameter, were too small to be resolved. We measured ϕ_L^{fl} by scanning the microscope's focal plane through a well-defined depth of approximately 100 μm and counting all of the large spheres with the aid of a charge-coupled device (CCD) camera, video recorder, frame grabber, computer, and NIH Image software. We used reference samples of known volume fractions to calibrate the relation between number of particles and volume fraction. In all cases, at least several hundred particles were imaged. These measurements gave ϕ_L^{fl} to within approximately 10%. We determined ϕ_S^{fl} by subtracting ϕ_L^{fl} from the total fluid-phase volume fraction. To determine the exact compositions of the solid phase, we had to assume a volume fraction of large spheres in the solid, ϕ_L^{sol}, as discussed in the following section.

To probe the structure of thick samples as phase separation occurred, we used diffusing-wave spectroscopy (DWS) [2] in the reflection geometry to measure the translational diffusivity of the particles. Typically, in DWS, when the motion of the scatterers is constrained (indicating a glass or solid structure), the intensity temporal autocorrelation function does not decay to zero. We mixed samples and measured the light-intensity autocorrelation function at various times. Immediately after mixing, DWS confirmed the fluid structure of the particles. When the intensity autocorrelation function no longer decayed to zero, we concluded that the sediment had become solid or glasslike. We used this technique to investigate the role of gravity in phase separation, as discussed in Sec. III A 2.

III. RESULTS

In this section, we describe the results of our experiments. In Sec. III A, we discuss our investigations of the nature of the sediment, the structures of the phases, formation of a gel, and the effect of gravity. In Sec. III B, the measured phase diagrams are presented for sphere-diameter ratios equal to 6.7, 8.8, and 12.0. In Sec. III C, we describe the structure of the surface phase, and finally, in Sec. III D, we discuss phase separation in mixtures with diameter ratio α as low as 2.0.

A. Detailed observations of the phase separation

Figure 2 represents the final phases of several binary samples which we observed over a period of one to four days after mixing. Initially, all samples were opaque white because the larger polystyrene spheres strongly scatter visible light. Some samples remained uniformly white for several days or weeks, until gravity induced settling of individual particles, and the sample was discarded. These samples were considered stable in the binary fluid phase (represented in Fig. 2 by a plus sign). In some samples, concentration fluctuations could be seen by eye minutes or hours after mixing. Subsequently, a well-defined interface could clearly be seen between a dilute fluid on the top and a more optically dense sediment on the bottom. Over a period of 12–48 h, this interface fell to the bottom of the sample (as described in more detail below). These were samples with bulk phase separation (represented by an asterisk in Fig. 2). In other samples, small spots on the surface of the cuvette became visible within approximately 12 h and no bulk interface was observed. These were samples with surface solidification only (open square). As α was increased, this surface-only region became narrower, nearly disappearing when $\alpha = 12.0$. The surface-phase measurements are discussed in Sec. III C. Other samples exhibited surface spots *and* bulk interfaces (open triangle). The lack of phase separation at the highest total volume fractions may have been caused by the slowing of the dynamics due to high viscosity.

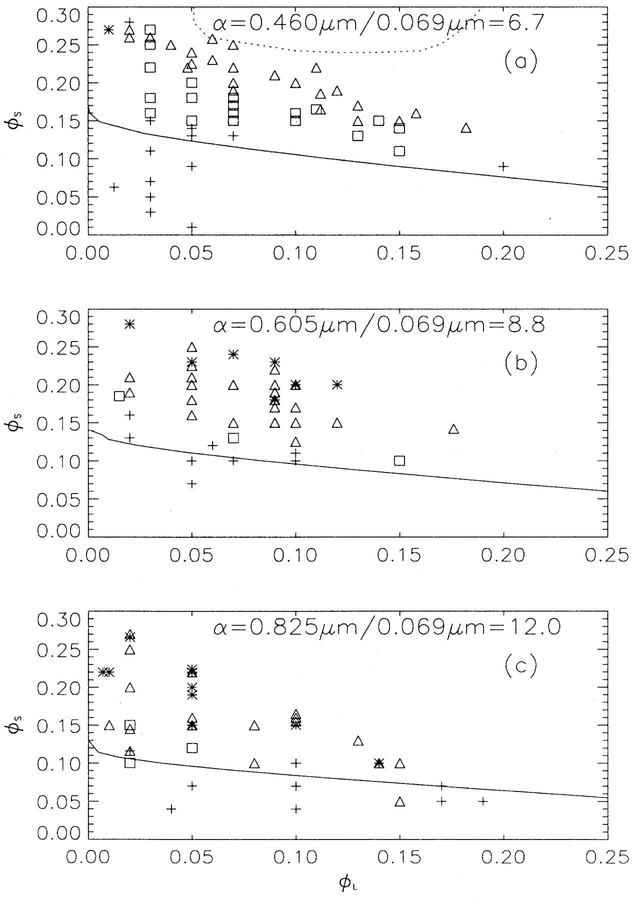

FIG. 2. Final phases of binary hard-sphere mixtures. The horizontal and vertical axes indicate the initial volume fractions of large and small spheres, respectively. Each symbol indicates a sample which we investigated and represents the phase behavior observed: +, no phase separation; □, growth of solid phase at surface; △, phase separation at surface and in bulk; *, fluid-solid phase separation in bulk only. The solid lines are liquidus curves derived in Sec. IV. The dashed curve in (a) represents the liquidus curve measured by Ref. [19] in suspensions of silica spheres with α= 6.

The liquidus curve separates the region of the phase space in which samples are homogeneous fluid in the bulk from the region in which samples have coexisting fluid and solid phases in the bulk. In Fig. 2, the measured liquidus curve (not drawn) separates the surface-solid–bulk-interface region from the region of stability in the binary fluid phase or the region of surface solidification. In the figure, we have plotted the liquidus curves calculated from the theory described in Sec. IV (solid curves). For comparison, the dashed curve in Fig. 2(a) represents the experimental results of van Duijneveldt *et al.* [19] who investigated mixtures of silica spheres with $\alpha = 6$, suspended in cyclohexane. They observed two-phase coexistence in samples above the dashed curve and a single bulk fluid phase in those below it. No surface phase was reported. The dashed curve should be compared to a curve separating the region of surface solidification from the surface-solid–bulk-interface region in the same figure. We observed phase separation at slightly lower ϕ_S, which is consistent with our slightly higher value of α, since the depletion energy is approximately proportional to $\alpha\phi_S$. van Duijneveldt *et al.*, however, find that the two-phase region has a high-ϕ_L boundary which we did not observe ($\phi_L \leq 0.20$). As pointed out in [19], the apparent high-ϕ_L boundary may be due to slow phase-separation dynamics in samples with relatively high particle concentrations. The relatively rapid gravitational settling (over a few hours) in these experiments prevented a definite characterization of the equilibrium structure of the second phase.

Optical microscopy indicated that the sediment is a concentrated suspension of either crystalline or glass clusters dispersed in the dilute fluid phase. The clusters contain from 20 (when $\phi_S \approx 0.30$) to 100 (ϕ_S near the liquidus curve) large spheres. In the higher-ϕ_S samples, these clusters rapidly formed a loose gel, as discussed in the following subsection. For several samples with a range of ϕ_S, we measured the total volume fractions (of large and small spheres) in the sediment to be 0.50–0.58. This volume fraction is consistent with a mixture of dense ($\phi_L + \phi_S \approx 0.74$) solid aggregates or crystallites comprising approximately 65% of the total sediment volume, with the surrounding fluid phase ($\phi_L + \phi_S \approx 0.2$)

comprising the rest of the sediment volume. Measuring the volume fractions in the sediment, therefore, does not accurately determine the volume fractions in the solid phase. In samples with ϕ_S within approximately 0.05 of the liquidus curve, the surface spots were strongly iridescent and the bulk sediment developed iridescent spots after a day or more. For the first day, the sediment in these samples would flow very slowly when the sample was tilted, after which time it would not flow to any visible extent. Possibly, neighboring crystallites in the sediment had begun to join, making the sediment more rigid. The early-time fluid nature of the sediment caused an earlier incorrect conclusion that the dense phase is a fluid instead of a solid [4].

In samples with ϕ_S within approximately 0.05 of the liquidus curve, optical microscopy of the solid phase showed that the large spheres were arranged in close-packed planes. The spheres in one plane always fit over the gaps in the neighboring planes. We concluded, however, that there were no long-range correlations among planes which would induce either face-centered cubic (fcc) or hexagonal close-packed (hcp) structure. We obtained a similar result for the surface crystals, as discussed in Sec. III C. There was no evidence of an ordered structure of small spheres either from scattering of light by bulk crystals or from scanning electron microscopy of the surface crystals.

1. Crossover from ordered to disordered dense phase

When ϕ_S was more than approximately 0.05 above the liquidus curve, the sediment exhibited no Bragg scattering and retained the ability to flow for several days. Large-sphere clusters were observed in these samples, but had structure significantly less well ordered than in samples with lower ϕ_S. With optical microscopy, it was not possible to recognize a regular crystal lattice in the solid phase of these samples. In samples with the highest α and ϕ_S (e.g., a_L/a_S=[0.825 μm]/[0.069 μm] = 12.0, $\phi_L =$ 0.02, and $\phi_S \geq 0.24$), the large spheres formed randomly packed clusters of approximately 20 particles within 10 min. Over the next 60 min, we observed these clusters fall to the bottom of the 100-μm-thick sample cell and form a loose gel of apparently fractal aggregates. With $\phi_S = 0.24$, these aggregates were as large as 75 μm across. Increasing ϕ_S by 0.02 increased the aggregate size to as large as 100 μm across.

We have observed a dramatic change in sedimentation behavior which further suggests a change in phase-separation dynamics as ϕ_S is changed. We videotaped five samples containing 0.605-μm and 0.069-μm spheres ($\alpha = 8.8$) with $\phi_L = 0.09$. In the sample with ϕ_S =0.15, an opaque sediment appeared at the bottom of the container and grew upward at approximately 1 cm/h, with no subsequent observable change in opacity. When ϕ_S was increased by just 0.02, another interface appeared at the top of the container and moved downward rapidly (approximately 2 cm/h). This interface separated the dilute fluid phase (on top) from a sediment which became more opaque as the interface fell. When $\phi_S \geq$0.19, only the top interface appeared. Increasing ϕ_S caused this interface to fall more slowly. We obtained similar results using samples with $\phi_L = 0.05$, with the second interface appearing when $\phi_S \geq 0.20$.

The above observations support the explanation proposed by Pusey *et al.* [28] of a similar crossover in the sedimentation behavior of mixtures of hard spheres with polymer. At low ϕ_S, the binary fluid is metastable, so that phase separation occurs by nucleation of ordered, dense crystallites which rapidly pile up at the bottom. In samples with higher ϕ_S, the depletion attraction between large spheres is sufficiently strong so that once they touch one another, they are unlikely to rearrange themselves to the lowest-free-energy structure and instead form a metastable disordered (glasslike) structure. Glass formation has also been observed in monodisperse hard-sphere colloids [7]. Our microscopic observations of the growth of fractal-like aggregates of large spheres indicate that the sediment is a gel. Pusey *et al.* [28] suggest that a slow rearrangement of the particles weakens the structure so that it collapses due to gravity, thus causing the interface to fall. According to our experiments, increasing ϕ_S causes the interface to fall more slowly, perhaps due to a slowing of the large-sphere rearrangement in the presence of a stronger depletion force and in the presence of a higher effective viscosity.

2. The effect of gravity on the equilibrium state

Although previous investigations of binary hard-sphere mixtures [19] have observed formation of crystals after several days, they could not rule out the possibility that a dense fluid of large spheres had formed, settled to the bottom, and become compressed by gravity to the point of solidification. To determine the effect of sedimentation on solidification, we prepared two samples (A and B) with the same volume fractions of large and small spheres. In sample A we replaced enough water with heavy water to make the polystyrene particles nearly neutrally buoyant. Thus, in sample A, the mass densities of water and polystyrene were the same within 0.5%, whereas in sample B they differed by 5.0%. We then measured the sedimentation rate of the bulk interface using time-lapse video. Simultaneously, we used DWS at regular intervals to determine when the sediment solidified (as discussed in Sec. II B). This typically occurred a few hours after the first visible signs of phase separation, but before the bulk interface had completely settled. We found that sample B settled approximately ten times faster than A, consistent with the mass densities. Sample B, however, solidified only two to four times faster than sample A, as determined by DWS. If solidification were *entirely* due to gravity, then the rate of solidification would scale with the rate of sedimentation. We found, however, that the solidification rate only *loosely* depended on sedimentation — gravity speeds up solidification, but is not required for the process. From the above evidence, we conclude that even in the absence of gravity, the bulk phases at equilibrium are a dilute binary fluid coexisting with a dense, ordered solid of large spheres in a close-packed lattice permeated by a fluid of small spheres.

B. Measured phase diagrams

In Fig. 3, we present experimental phase diagrams for three sphere-diameter ratios (α = 6.7, 8.8, and 12.0). In each diagram, the solid line represents the bulk liquidus, determined by observing which samples had coexisting fluid and solid phases in the bulk and which did not (i.e., by drawing a curve between the open triangle and the plus sign or open square of Fig. 2). As α is increased, the liquidus curves move to lower ϕ_S. Thus increasing α makes the fluid phase thermodynamically unstable at lower ϕ_S, as expected from the simple model in which the energy of the depletion attraction is proportional to $\alpha\phi_S k_B T$ [12]. For comparison, we also plot the bulk phase diagram calculated from the theory described in Sec. IV. The measured liquidus agrees closely with the calculated liquidus at the higher values of α, as discussed in Sec. IV.

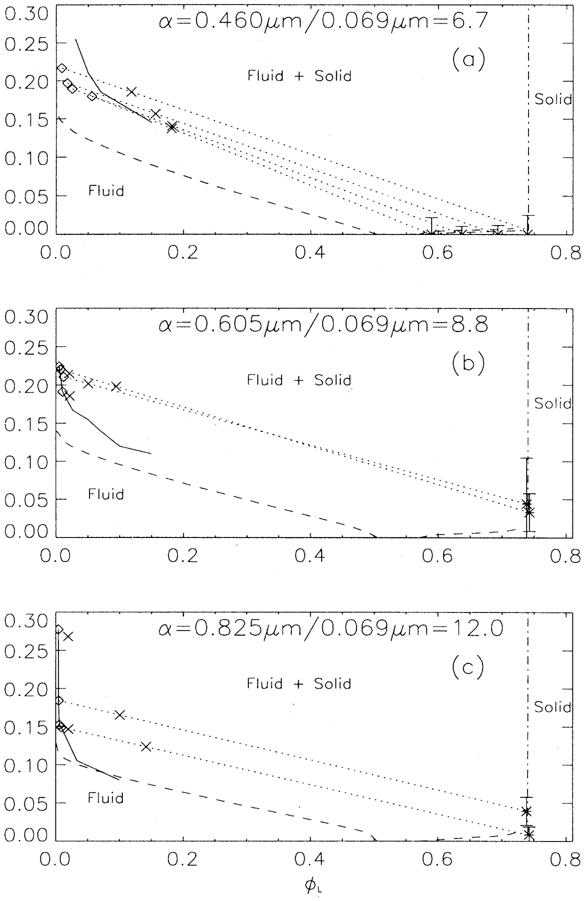

FIG. 3. Experimentally determined phase diagrams. The × represent the initial volume fractions (before phase separation) and the ◇, represent the measured volume fractions in the fluid phase at equilibrium. The dotted lines represent measured tie lines, determined by the ◇ and ×. The end points of the tie lines must lie on the liquidus and solidus curves (the disagreement in (a) is discussed in section III B). The measured bulk liquidus curves, determined from the data in Fig. 2, are represented by the solid lines. The estimated solidus curves (corresponding to the upper bound for ϕ_L^{sol}, as discussed in Sec. III B) are represented by the dot-dashed lines. The error bars represent the uncertainties in the extrapolated ϕ_S^{sol}. Errors for the ◇ and × are smaller than the plot symbols. All of these results are listed in Table I. The dashed curves represent the liquidus and solidus curves derived from the theory of Sec. IV.

For several samples, we measured the volume fractions in the fluid phase at equilibrium, ϕ_L^{fl} and ϕ_S^{fl}, using the method described in Sec. II B. The results of these measurements are listed in Table I and plotted in Fig. 3. The multipication symbols represent the volume fractions immediately after mixing, while the open diamonds represent the volume fractions in the fluid phase, ϕ_L^{fl} and ϕ_S^{fl}, measured two days after the samples were mixed (after which no further changes in the sediment were observable). In the absence of phase separation at the surface, the equilibrium-fluid-phase volume fractions (open diamonds) must lie on the bulk liquidus curve. In samples with α = 6.7, however, the open diamonds lie *below* the bulk liquidus curve. In these samples, the growth of crystallites on the surface of the container reduces the equilibrium values of ϕ_L^{fl}. Due to these surface crystals, the equilibrium ϕ_L^{fl} and ϕ_S^{fl} (open diamonds) should lie along the boundary between the homogeneous-fluid region and surface-solid-only region, i.e., between the plus signs and the open squares of Fig. 2. The open diamonds lie in the middle of the surface-solid-only region, however, indicating that these samples had not yet reached equilibrium with respect to the surface-phase separation when we made the measurements. We decanted the samples after two days to avoid the effects of gravitational settling of individual particles. According to our observations of similar samples, however, the surface crystals continue to grow for at least two weeks and sometimes for several months. In these samples, therefore, the large spheres may still have been in the process of crystallizing on the surface. Repeating the measurements with two-week-old samples would likely give slightly lower ϕ_L^{fl} (even if gravitational settling could be eliminated). In samples with α = 8.8 and 12.0, the surface-phase-only region is very narrow, so that the measured ϕ_L^{fl} and ϕ_S^{fl} are very close to the bulk liquidus curve. We always found large spheres in the fluid phase, indicating that only a fraction of the large spheres solidified. For given initial volume fractions, however, increasing the size asymmetry caused more large spheres to separate out of the fluid. For example, with initial ϕ_L/ϕ_S = 0.10/0.19, increasing α from 6.7 to 8.8 increased the relative number of large spheres in the solid from 85% to 90%.

We next considered the composition of the solid phase, ϕ_S^{sol} and ϕ_L^{sol}. The sediment which falls to the bottom of the sample container during phase separation is a *mixture* of the solid and fluid phases. Therefore measurements of its composition do not determine the volume fractions in the solid, although they do provide a lower bound of

TABLE I. Table of measured and extrapolated volume fractions of the phases at equilibrium in samples with $\alpha = 6.7$, 8.8, and 12.0. The initial and equilibrium-fluid-phase volume fractions were measured directly. The last two columns list the upper limits for ϕ_L^{sol} and the corresponding values of ϕ_S^{sol} in each sample, calculated from the data in the third and fourth columns. For some samples, the extrapolated solid-phase compositions are not listed because the error bars for the extrapolated ϕ_S^{sol} are very large, approximately ±0.20. The same data are plotted in Fig. 3.

Sample	a_L (μm)/ a_S(μm)	Init. $\phi_L/\phi_S(\pm 1\%)$	Measured ϕ_L^{fl} / ϕ_S^{fl}	ϕ_L^{sol}	ϕ_S^{sol}
1	0.460 / 0.069	0.1810 / 0.1374	0.0556±0.0054 / 0.1796±0.0059	0.589	0.00±0.022
2	=6.7	0.1818 / 0.1408	0.0251±0.0019 / 0.1893 ±0.0029	0.637	0.00± 0.011
3		0.1558 / 0.1566	0.01719±0.00066 / 0.1970±0.0022	0.693	0.00±0.012
4		0.1179 / 0.1853	0.0087±0.0013 / 0.2168±0.0026	0.7405	0.0055±0.0196
5	0.605 / 0.069	0.0944 / 0.1981	0.00709±0.00086 / 0.2204±0.0024	0.7405	0.033±0.025
6	=8.8	0.0215 / 0.1857	0.0102±0.0011 / 0.1912±0.0023		
7		0.0506 / 0.2018	0.0120±0.0013 / 0.2106±0.0026	0.7405	0.0441±0.0606
8		0.0210 / 0.2151	0.0050±0.0006 / 0.2243±0.0024		
9	0.825 / 0.069	0.0196 / 0.1468	0.00538±0.00063 / 0.1526±0.0017		
10	=12.0	0.1417 / 0.1236	0.00856±0.00072 / 0.1492±0.0017	0.7405	0.0084±0.0105
11		0.1003 / 0.1653	0.00452±0.00055 / 0.1842±0.0020	0.7405	0.039±0.018
12		0.0191 / 0.2682	0.0039±0.0005 / 0.2775±0.0029		

between 0.50 and 0.58 for $\phi_L^{sol} + \phi_S^{sol}$. To determine the composition of the solid phase, we plot a straight line between $(\phi_L^{fl}, \phi_S^{fl})$ and (initial ϕ_L, initial ϕ_S). This "tie line" indicates the equilibrium state of any mixture with initial volume fractions given by a point along the tie line. Such a sample will separate into two phases whose compositions are given by the tie line's end points, which lie on the liquidus and solidus curves. The relative volume of each phase is inversely proportional to the distance from the initial point to the corresponding end of the tie line. To determine uniquely the composition of the solid phase from the tie line, we must assume a value for either ϕ_L^{sol} or ϕ_S^{sol}. The *upper* bound for ϕ_L^{sol} is determined by the geometry of packing the spheres: $\phi_L^{sol} \leq 0.7405$. For the three samples numbered 1, 2, and 3 in Table I, however, assuming $\phi_L^{sol} = 0.74$ leads to negative ϕ_S^{sol}. Therefore these three samples, which have the lowest values of α and ϕ_S, must have $\phi_L^{sol} < 0.74$, i.e., the large spheres in the lattice do not touch one another. For these samples, the upper bound for ϕ_L^{sol} is determined by the intersection of the tie line with the ϕ_L axis. The dashed line in Fig. 3 represents the solidus curve obtained using these upper limits for ϕ_L^{sol}. The corresponding values for ϕ_S^{sol}, listed in Table I, range from 0 to 0.04±0.06. Only in sample number 11 does ϕ_S^{sol} not equal zero within the experimental uncertainty. These results agree, within experimental uncertainties, with calculations using the theory described in Sec. IV. We determine the *lower* bound for ϕ_L^{sol} of all of the samples in the following way. Because sample number 1 has the lowest α and initial ϕ_S (therefore the weakest depletion force pulling the large spheres together), it is likely to have the lowest ϕ_L^{sol}. For this sample, the lower bound for $\phi_L^{sol} + \phi_S^{sol}$ is 0.57±0.02, obtained by analyzing the sediment as mentioned above. Applying this condition to the measured tie line, we find that $\phi_L^{sol} \geq 0.55$. A similar analysis applied to sample number 2 (for which the total volume fraction of polystyrene in the sediment is 0.58±0.02) gives the condition $\phi_L^{sol} \geq 0.56$. All of the other samples which we studied had larger α or ϕ_S, and are therefore assumed to have $\phi_L^{sol} > 0.56$. The upper bounds for ϕ_S^{sol} are obtained by setting ϕ_L^{sol} to its minimum value, 0.56. The largest value of ϕ_S^{sol} thus obtained is 0.09±0.05, evident from the tie lines in Fig. 3. Finally, the minimum value of ϕ_L^{sol}, 0.56, obtained for the $\alpha = 6.7$ system corresponds to a distance between large spheres of less than $a_L + a_S$, as expected from the theory of the depletion force.

C. Crystallization on the surface of the sample container

As previously reported [4], we often observed iridescent spots growing on the walls of the container, even in samples that were stable in the bulk. Such samples are marked with open squares in Fig. 2. Optical microscopy of these spots revealed crystallites thought to have formed due to the depletion attraction, as described in the Introduction and in Ref. [4]. The crystals had domains of hexagonally ordered large-sphere planes aligned parallel to the wall. Each crystallite had many such domains, which ranged in size from five to 500 large spheres per plane, with the larger domains and larger crystallites always appearing in samples with lower ϕ_S. The crystallites' thickness consistently varied from one or two layers, at high α and/or high ϕ_S, to approximately 100 layers, at lower α and ϕ_S. We measured the thickness by optical microscopy, by inspection of the crystallites from both sides of a 1-mm-thick sample, and by addition of enough salt to the system to cause rapid, irreversible flocculation which allowed the surface crystallites to be removed from the surrounding fluid and inspected. Due to the strong scattering of visible light, we were unable to see far enough into the sample to determine directly the sequence of plane stacking normal to the cell wall. The symmetry of Kossel-scattering patterns [3] and measurements of spacings in various crystallographic directions (using scanning electron microscopy), however, ruled out body-centered cubic (bcc) structure and suggested random stacking of close-packed planes [29]. Our results indicate that the surface crystalline phase has the same structure as the bulk crystalline phase, with similar concentrations of small spheres and a similar decrease in large-sphere order with increasing ϕ_S.

A theoretical model for growth of the solid phase on the surface of the sample container has been published by Poon and Warren [10]. In this model, the surface solid phase is assumed to be only a single layer thick. This model predicts surface fluid-solid coexistence only along a single line in the phase diagram, above which the surface is completely covered by the solid phase. According to our experiments, however, the solid phase always grows several layers in thickness and coexists with the surface fluid in a *region* of the phase diagram (represented by the open squares and open triangles in Fig. 2). The solid phase covers approximately 1–50 % of the surface, with the more complete coverage observed in samples with higher ϕ_S.

We have also observed a dense fluid of large spheres wetting the surface, consistent with the depletion-force model of Ref. [4]. This fluid surrounds the surface crystallites in samples in which they appear. Even in samples with low ϕ_S, in which no crystals are observed, ϕ_L at the surface is increased over the bulk value by a factor of up to approximately 5. For example, in a neutrally buoyant sample with a_L/a_S=[0.605 μm]/[0.069 μm] = 8.8, ϕ_L/ϕ_S = 0.015/0.185, no crystals appeared but, within minutes, ϕ_L increased to approximately 0.06 along the wall (measured by optical microscopy). Each large sphere diffused along the surface for an average of several minutes before diffusing back into the bulk [30]. In monodisperse samples with the same ϕ_L (ϕ_S=0), the large spheres stayed on the surface for an average of only approximately one second. Samples in which only the dense surface *fluid* appeared are not represented in Fig. 2. In samples with sufficiently high ϕ_S (indicated by the open square in Fig. 2), we observed the nucleation of crystallites in this surface fluid. Further investigations of the crystallite-nucleation process at the surface will be published [31].

D. Crystallization in samples with low diameter ratios

We have observed surface crystallization and bulk separation into a fluid plus a crystalline or glass phase in samples with α as low as 2.0 and $\phi_L + \phi_S$ as low as 0.35. [There are intriguing geometric constraints on these low-α crystals. If the large spheres are touching and if $\alpha >$ 6.4, then the small particles can flow freely (like a gas) through the interstices. If $2.4 < \alpha < 6.4$, the small particles would be trapped in the large-sphere interstices. If $\alpha <$2.4, the small spheres would not fit anywhere inside the large-sphere crystal.] The results are summarized in Table II. All of the surface crystallites have a three-fold symmetry normal to the wall, similar to the higher-α samples. Using DWS, we determined that the sediment had a solid or glass structure similar to the higher-α samples described above. Recent theoretical approaches have predicted a spinodal instability in binary hard-sphere fluids with α greater than approximately 4 [15] or 5 [14].

Two-fluid coexistence was not observed, in contrast to some theoretical models which predict a fluid-fluid phase separation in mixtures of hard spheres and polymer with α < 3 [9,26]. Two-fluid coexistence has been observed in hard-sphere–polymer mixtures [21,23] with α (using the polymer radius of gyration or hydrodynamic radius) = 3.0, 4.0, and 4.75. For α = 2.0 and 3.0, we observed

TABLE II. Table of results for $\alpha \leq 4.6$. Results for samples with α= 6.7, 8.8, and 12.0 are plotted in Fig. 2. The phase behavior column describes our observations: "-"indicates no observed phase separation of any type, and "surface" and "bulk" indicate phase separation into fluid and solid phases at the container wall and in the bulk of the sample, respectively. No fluid-fluid separation was observed.

$a_L(\mu\text{m})/a_S(\mu\text{m})$	$\alpha \equiv a_L/a_S$	ϕ_L / ϕ_S	Observed phase behavior
0.299 / 0.065	4.6	0.05 / 0.17	-
		0.05 / 0.25	-
		0.05 / 0.30	-
		0.05 / 0.40	-
		0.07 / 0.29	surface
		0.07 / 0.35	-
		0.10 / 0.19	-
0.460 / 0.137	3.4	0.05 / 0.16	-
		0.05 / 0.26	-
0.204 / 0.069	3.0	0.03 / 0.10	-
		0.05 / 0.05	-
		0.05 / 0.25	-
		0.15 / 0.15	-
		0.18 / 0.19	bulk, surface
		0.23 / 0.22	bulk, surface
0.605 / 0.296	2.0	0.25 / 0.18	-
0.137 / 0.069	2.0	0.18 / 0.18	-
		0.15 / 0.27	surface
		0.22 / 0.20	bulk, surface
		0.28 / 0.07	bulk, surface

single-fluid and fluid-solid regions, with no two-fluid region in between. It is possible, however, that fluid-fluid separation in binary hard-sphere mixtures appears in the narrow range of volume fractions which we happened to miss.

IV. THEORETICAL MODEL

In this section we calculate the phase diagram for the binary hard-sphere system with $\alpha > 6.4$. For the solid phase, we employ a simple model [5] to calculate the Helmholtz free energy with no arbitrary parameters. To calculate the free energy of the binary fluid phase, we use the well-known equation of state due to Carnahan and Starling [32] with modifications. Our model predicts fluid-solid phase transitions in monodisperse hard-sphere colloids, in close agreement with the results of computer simulations. We also predict fluid-solid phase separation in binary mixtures, in agreement with our measurements.

It is constructive to compare our approach to that of Poon and Warren [10] (who follow the approach of Refs. [8,9]). Both approaches predict coexistence of a binary fluid and a close-packed lattice of large spheres permeated by a dilute fluid of small spheres. To determine the free energy of the large spheres in the fluid phase, both rely on the equation of state due to Carnahan and Starling [32]. Also, both assume that the small particles reside in a reduced volume which depends on the volume fraction of the large spheres. There are, however, significant differences. First, in Refs. [9,10], the reduced volume in which the small particles reside, in both the fluid and solid phases, is determined by comparison of the chemical potential of an ideal gas of small particles in the reduced volume to the chemical potential of the small particles in a binary hard-sphere fluid, calculated within the Percus-Yevick approximation. In the present approach, this reduced volume is calculated using simple geometric arguments. Second, for the large-sphere crystal, Refs. [10,9] use the results of a computer simulation, whereas the present approach derives the free energy analytically, following Buehler *et al.* [5]. The latter method has the advantage of calculating the chemical potential without unknown additive constants. Finally, the present approach does not *a priori* assume phase separation in a monodisperse mixture with ϕ approximately 0.5. Instead, this behavior is predicted. The phase diagrams calculated within these two approaches agree reasonably well, as shown in Fig. 6(a).

The equilibrium conditions for colloids (which are of constant total volume and in contact with a heat reservoir, the room) are obtained by minimizing the Helmholtz free energy F with respect to all free parameters. In particular, the osmotic pressures of the two phases are set equal, and the chemical potential of large (small) spheres in the fluid phase is set equal to that of the large (small) spheres in the solid phase. We solve the resulting equations to determine the volume fractions of the fluid and solid phases which coexist at equilibrium.

We omit the water from considerations of the particle thermodynamics. Water plays an important role in the particle dynamics, and it keeps the particles suspended, but its free energy does not depend on the arrangement of the colloidal spheres. Therefore it has no effect on the equilibrium colloidal structure.

For the fluid and solid phases, we divide the total Helmholtz free energy into two pieces: one due to the large spheres (denoted by the subscript L) and one due to the small spheres (denoted by the subscript S). Thus $F^{fl}_{total} = F^{fl}_L + F^{fl}_S$ and $F^{sol}_{total} = F^{sol}_L + F^{sol}_S$. The superscripts fl and sol denote fluid and solid phase, respectively.

A. Large-sphere crystal

We explicitly calculate the free energy of the crystal of large spheres. Since there is no interaction between the spheres when they are not touching, we do not rely on harmonic-solid approximations. Instead, we use the method of Buehler *et al.* [5], who consider each sphere to move freely in a hard "cage" formed by its nearest neighbors, which are assumed to lie on a lattice (see Fig. 4). In this mean-field approach, the effect of lattice fluctuations on the cage volumes is neglected. The volume of the cage, v^*, is equal to the volume accessible to the center of mass of each sphere in the lattice. We do not subtract from v^* the volume of the small particles, since they are excluded from much of the volume which is available to the large spheres [see Fig. 1(b)]. Therefore the free energy of the large-sphere crystal is independent of the small-sphere volume fraction. The energy of the crystal is just the kinetic energy, $p^2/2m$, where p and m are the momentum and mass of each sphere. The partition function Z and Helmholtz free energy F^{sol}_L can therefore be calculated.

$$Z = \left\{ \frac{1}{(2\pi\hbar)^{\frac{3}{2}}} \int_{v^*} d^3r \int d^3p \, \exp\left(-\frac{p^2}{2mk_BT}\right) \right\}^{N_L}, \quad (1)$$

$$\frac{F^{sol}_L}{k_BT} = -\ln Z = -N_L \ln v^* + 3N_L \ln \Lambda, \quad (2)$$

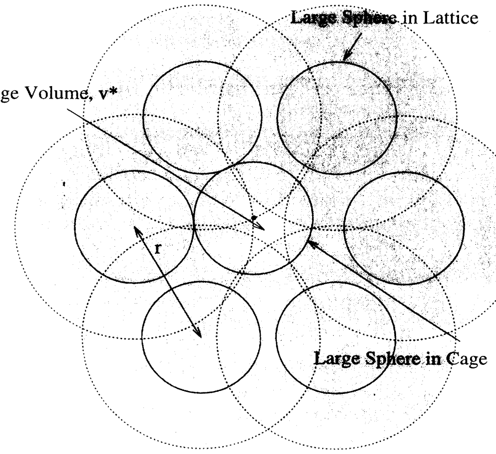

FIG. 4. Diagram of the large-sphere crystal. Due to the hard-core repulsion, the middle sphere's center of mass can fit only in the small central white region which is a two-dimensional slice of the cage volume, v^*.

where k_B, T, and N_L are Boltzmann's constant, temperature, and number of large spheres in the solid, respectively. The thermal wavelength Λ is defined as $\Lambda \equiv \sqrt{2\pi\hbar^2/(mk_BT)}$, where $\hbar$ is Planck's constant. This equation for the partition function Z differs from the ideal-gas result in two ways: the spatial integral is limited to the cage volume v^*, and the factor $1/N_L!$ is omitted in order to make F_L^{sol} extensive. (Since each large sphere is uniquely associated with a particular cage, the spheres are distinguishable.)

To calculate v^* as a function of lattice spacing, we divide space into small voxels and use a computer to count the number of voxels in which the center of a large sphere can reside without that sphere's overlapping any neighbors. The values of v^* for fcc and hcp structures are identical. We fit a polynomial to the results of our calculation:

$$\begin{aligned}\frac{v^*}{a^3} = 6.733 \times 10^{-7} \left(\frac{r}{a} - 1\right) - 4.313 \times 10^{-4} \left(\frac{r}{a} - 1\right)^2 \\ +4.809 \left(\frac{r}{a} - 1\right)^3, \end{aligned} \tag{3}$$

where r is the distance between the centers of neighboring spheres in the lattice and a is the sphere diameter. This polynomial deviates from the computer results by less than 3% when $\phi > 0.56$. In the calculated phase diagram, ϕ is always greater than 0.56. We find that varying v^* by 10% has a less than 1% effect on the calculated coexisting volume fractions in the monodisperse case.

In Fig. 5, we compare the osmotic pressure $(-\partial F/\partial V)$ of the monodisperse hard-sphere crystal calculated in Ref. [5], as described above, to the results of a fit by Hall to computer simulation results [Eq. (13) of Ref. [33]]. The agreement indicates that the cage model provides a reasonably accurate understanding of the hard-sphere crystal, although it appears to underestimate the solid-phase pressure by as much as 7% when $\phi = 0.57$, perhaps due to neglecting fluctuations. Agreement improves with increasing ϕ, except very near closest packing, at which point the pressure diverges.

B. Fluid structures

We model the small and large spheres in the fluid phase and the small spheres in the solid phase as hard-sphere fluids existing in *effective* volumes, as defined below. The hard-sphere-fluid free energy is obtained by integration of the Carnahan-Starling (CS) equation of state for a monodisperse hard-sphere fluid [32],

$$\frac{P^{\mathrm{CS}}V}{Nk_BT} = \frac{1+\phi+\phi^2-\phi^3}{(1-\phi)^3}. \tag{4}$$

$$\begin{aligned}\frac{F}{k_BT} &= -\int_0^V \frac{P(N,T,V')}{k_BT} dV' \\ &= \frac{V}{\pi a^3/6}\left(\frac{3\phi-2\phi^2}{(1-\phi)^2} + \phi \ln \phi\right) + \frac{F_0(N,T)}{k_BT}, \end{aligned} \tag{5}$$

where P is the fluid osmotic pressure, V is the total volume of the fluid phase, a is the sphere diameter, N is the number of spheres, ϕ is the volume fraction of spheres ($\phi \equiv N\pi a^3/6V$), and F_0 is the integration constant, independent of V. The Carnahan-Starling equation of state deviates from results of molecular dynamics simulations by less than 0.5% when $\phi < 0.49$.

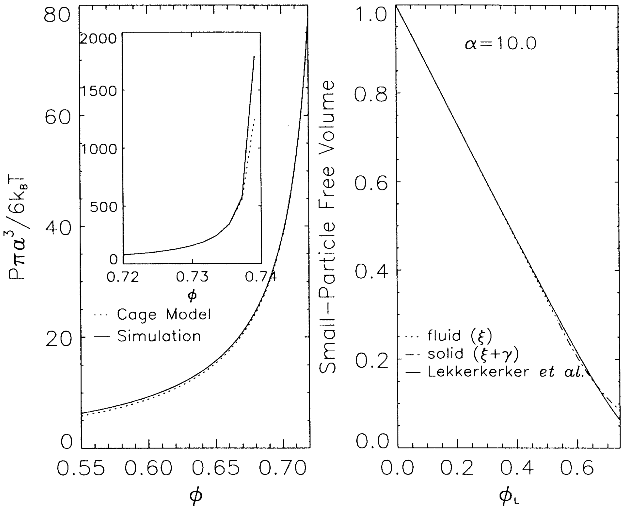

FIG. 5. Left — plot of the osmotic pressure of a monodisperse hard-sphere fcc or hcp crystal as a function of volume fraction of spheres. The dotted line represents the results of the calculation described in the text and in [5], while the solid line represents the results of Hall [33], from a fit to computer-simulation results. There are no free parameters. Right — the fractional volume accessible to the small particles as a function of large-sphere volume fraction. The dotted and dashed lines show the results of the present approach, Eqs. (8) (for fluid phase, with $\phi_L < 0.55$) and (9) (for solid phase, with $\phi_L \geq 0.55$). The solid line shows the result of Ref. [9], Eq. (9).

The centers of the small spheres are excluded from the interior of shells of diameter $a_L + a_S$ centered at each large sphere (see Fig. 1). Therefore the *effective* small-sphere volume fractions in the fluid and solid phases ($\widetilde{\phi}_S^{fl}$ and $\widetilde{\phi}_S^{sol}$) are greater than the real volume fractions:

$$\widetilde{\phi}_S^{fl} \equiv \frac{N_S\pi a_S^3/6}{\xi V} = \frac{\phi_S^{fl}}{\xi}, \tag{6}$$

$$\widetilde{\phi}_S^{sol} \equiv \frac{N_S\pi a_S^3/6}{(\xi+\gamma)V} = \frac{\phi_S^{sol}}{(\xi+\gamma)}, \tag{7}$$

where ξV and $(\xi+\gamma)V$ (defined below) are the volumes accessible to the centers of mass of the small spheres in the fluid and solid phases, respectively. Although these quantities depend on the number and positions of the large spheres, in a mean-field approach they are assumed to depend only on ϕ_L. In the fluid phase, the accessible volume is the total volume minus the excluded-volume spheres of diameter $a_L + a_S$:

$$\xi = \frac{1}{V}\left(V - N_L\frac{\pi}{6}(a_L+a_S)^3\right) = 1 - \phi_L^{fl}\left(1+\frac{1}{\alpha}\right)^3. \tag{8}$$

In the solid (i.e., for $\phi_L \gtrsim 0.5$), the large spheres are close enough together so that the excluded-volume regions overlap [see Fig. 1(b)], thus *increasing* the volume accessible to the small-sphere centers of mass by the amount γV, and increasing the small spheres' entropy. Thus the term γ may be thought of as representing the driving ("depletion") force of the phase separation.

$$\gamma = (N^{bonds})\frac{N_L}{V}V^{overlap} = 6\phi_L\left(1+\frac{1}{\alpha}-\frac{r}{a_L}\right)^2\left(1+\frac{1}{\alpha}+\frac{r}{2a_L}\right), \qquad (9)$$

where $V^{overlap}$ is the volume of the region of overlap of the two excluded-volume spheres (heavily shaded region in Fig. 1) and r is the separation between large-sphere centers in the lattice, $r/a_L = (0.7405/\phi_L)^{1/3}$. N^{bonds} is the number of "bonds" for each large sphere in the lattice, equal to half the number of nearest neighbors. For the close-packed lattice considered here, $N^{bonds} = 6$. In Fig. 5, we compare the volume accessible to the small spheres in the present theory to the free volume accessible to the small particles in the theory of Lekkerkerker *et al.* [9]. The two results agree closely except near closest packing, where the present theory predicts a 40% larger free volume, corresponding to lower crystal free energy.

Similarly, we define an effective volume fraction $\widetilde{\phi}_L^{fl}$ for the large spheres in the fluid phase. The volume accessible to the centers of the large spheres is λV, where λ accounts for the presence of the small spheres.

$$\widetilde{\phi}_L^{fl} \equiv \frac{N_L\pi a_L^3/6}{\lambda V} = \frac{\phi_L^{fl}}{\lambda}, \qquad (10)$$

$$\lambda = \frac{1}{V}(V - N_S\pi a_S^3/6) = 1 - \phi_S^{fl}. \qquad (11)$$

Finally, to obtain F_L^{fl}, F_S^{fl}, and F_S^{sol}, we write the fluid free energy of Eq. (5) in terms of the effective volume fractions $\widetilde{\phi}_L^{fl}, \widetilde{\phi}_S^{fl}$, and $\widetilde{\phi}_S^{sol}$. The osmotic pressure for each phase is given by the negative of the derivative of the total free energy with respect to volume. The chemical potentials are calculated by taking the derivative of the total free energy with respect to particle number, keeping in mind that $\widetilde{\phi}_S$ depends on N_S *and* on N_L. Differentiation of the integration constant, $F_0(N,T)$ of Eq. (5), results in an additive constant μ_0 in the chemical potential. Since the small spheres are a fluid in both phases, $\mu_{0,S}$ is the same in both solid and fluid phases and cancels out when the chemical potentials are set equal. For the large spheres, however, $\mu_{0,L}$ is different in the two phases. While μ_L^{sol} is completely determined by Eq. (2), we determine $\mu_{0,L}^{fl}$ by requiring that the chemical potential of the large spheres ($\phi_S = 0$) equal that of an ideal gas of large spheres as $\phi_L \to 0$. This extrapolation to the ideal-gas result gives $\mu_{0,L}^{fl} = \ln(6\Lambda^3/\pi a^3) - 4$.

C. Equilibrium conditions

For convenience, we define a dimensionless pressure, Π, which is the Carnahan-Starling pressure times the volume of a particle divided by k_BT:

$$\Pi(\phi) \equiv \frac{P^{\mathrm{CS}}\pi a^3/6}{k_BT} = \left(\frac{\phi+\phi^2+\phi^3-\phi^4}{(1-\phi)^3}\right). \qquad (12)$$

The total osmotic pressures, $P(\pi a_L^3/6)/(k_BT)$, in the fluid and solid phases must be equal:

$$\alpha^3\Pi(\widetilde{\phi}_S^{fl}) + \Pi(\widetilde{\phi}_L^{fl}) = -(\phi_L^{sol})^2\frac{\partial \ln v^*}{\partial\phi_L^{sol}} + \alpha^3\Pi(\widetilde{\phi}_S^{sol}) \times \left(\xi+\gamma-\phi_L^{sol}\frac{\partial(\xi+\gamma)}{\partial\phi_L^{sol}}\right). \qquad (13)$$

The fluid pressure [left-hand side of Eq. (13)] is simply the sum of the pressures of the large and small particles in their effective volumes. In the solid-phase pressure (right-hand side), the first term represents the change of large-sphere free energy with volume, while the second term represents the effect that changes in the lattice spacing have on the volume accessible to the small spheres, weighted by the pressure exerted by the small spheres.

The small-sphere chemical potentials, μ_S/k_BT, must be equal:

$$\frac{4-4\widetilde{\phi}_S^{fl}+3(\widetilde{\phi}_S^{fl})^2-(\widetilde{\phi}_S^{fl})^3}{(1-\widetilde{\phi}_S^{fl})^3} + \ln\widetilde{\phi}_S^{fl} + \frac{1}{\alpha^3}\Pi(\widetilde{\phi}_L^{fl}) = \frac{4-4\widetilde{\phi}_S^{sol}+3(\widetilde{\phi}_S^{sol})^2-(\widetilde{\phi}_S^{sol})^3}{(1-\widetilde{\phi}_S^{sol})^3} + \ln\widetilde{\phi}_S^{sol}. \qquad (14)$$

The chemical potential in the fluid phase [left-hand side of Eq. (14)] has two terms due purely to the small spheres in addition to a term, weighted by the large-sphere pressure, which accounts for the change in volume accessible to the large spheres when more small spheres are added. The solid phase lacks the latter term because F_L^{sol} does not depend on the small-sphere concentration. Because the chemical potential does not have the same functional form in both phases, the reduced small-sphere volume fractions are not quite equal at equilibrium.

Finally, the large-sphere chemical potentials, μ_L/k_BT, must be equal:

$$\frac{4-4\widetilde{\phi}_L^{fl}+3(\widetilde{\phi}_L^{fl})^2-(\widetilde{\phi}_L^{fl})^3}{(1-\widetilde{\phi}_L^{fl})^3} + \ln\widetilde{\phi}_L^{fl} - 4 - \alpha^3\frac{\partial\xi}{\partial\phi_L^{fl}}\Pi(\widetilde{\phi}_S^{fl}) = -\ln\frac{v^*}{\pi a_L^3/6} - \alpha^3\frac{\partial(\xi+\gamma)}{\partial\phi_L^{sol}}\Pi(\widetilde{\phi}_S^{sol}). \qquad (15)$$

Here, the terms involving the derivatives of the free-volume coefficients account for the dependence on ϕ_L^{sol} of the volume accessible to the small spheres. The -4 in the fluid-phase chemical potential comes from $\mu_{0,L}^{fl}$, defined above. We numerically solved these three equations for the volume fractions of coexisting phases at equilibrium. In Fig. 3, the calculated phase diagrams are presented along with the experimental data.

Our results for the monodisperse case (ϕ_S=0) agree closely with the results of computer simulations and experiments [7]. We predict the coexisting fluid and solid volume fractions to be 0.505 and 0.569, while the corresponding numbers from the computer simulations are 0.494 and 0.545. The theoretical phase diagrams also agree reasonably well with our experimental results for binary mixtures, especially for the higher values of α. When $\alpha < 10$, our measurements generally show that the solid phase is more difficult to form than predicted (i.e., it forms at higher ϕ_S than predicted). This trend may be due to the increased confinement of the small spheres as α is reduced. Although our model does account for the reduced volume available to the small spheres, we ignore the *shape* of this accessible volume, which becomes increasingly convoluted as α decreases. This effect could increase the free energy of the small spheres in the solid. Our assumption that the crystal contains no defects probably also underestimates the free energy, since the observed crystals had many such defects. Both of these effects could cause the present model to predict phase separation at volume fractions lower than those observed. The relatively large disagreement of theory and experiment for $\alpha = 6.7$ is at least partly due to the fact that the bulk-phase separation is preempted by the surface-phase separation. Our model predicts only the concentrations for which the bulk solid is stable with respect to the bulk fluid—we do not predict whether this bulk phase is metastable with respect to the surface solid. Possibly, in the region shown by open squares in Fig. 2(a), the surface solid phase forms and reduces ϕ_L in the bulk enough to make the bulk fluid phase stable. Finally, the slight nonideality of the polystyrene spheres could explain the disagreement. The theory predicts that 0.805-μm-large spheres in the solid phase could lie within 5 nm of one another. At such close range, the polystyrene spheres used in our experiments begin to repel one another due to the charges on the surfaces, thus competing with the depletion attraction. A correction for this effect could be incorporated into the model by including this interaction energy in the solid-phase free energy.

The effect on the phase diagram due to the small particles' hard-core repulsion is revealed by a comparison of the results of the present approach to that of Lekkerkerker *et al.* [9], who consider mixtures of hard spheres with polymer. In the latter approach, the small particles are treated as an ideal gas, which has a pressure lower than that of a hard-sphere fluid of the same volume fraction. As expected, the increased pressure exerted by the small spheres widens the fluid-solid coexistence region, as shown in Fig. 6(b). In particular, with $\alpha = 10.0$, the hard-core repulsion of the small spheres lowers the values of ϕ_S along the liquidus curve by a factor of approximately 2.

V. CONCLUSIONS

We have determined the structures and compositions of the phases of binary mixtures of polystyrene particles which closely resemble hard spheres. An experimentally derived phase diagram for systems with $12.0 > (a_L/a_S) > 6.7$ was presented. We understand these results using a simple intuitive model whose predictions agree reasonably well with the experimental results. We have discussed the effects of gravity and dynamics of phase separation on the structure and sedimentation of the phases. Measurements of the structure of the crystalline phase growing on the surface of the container suggest it is a wetting of the bulk crystalline phase. We are pursuing further investigations of nucleation of these surface crystallites in the large-sphere fluid which wets the surface even at very low volume fractions.

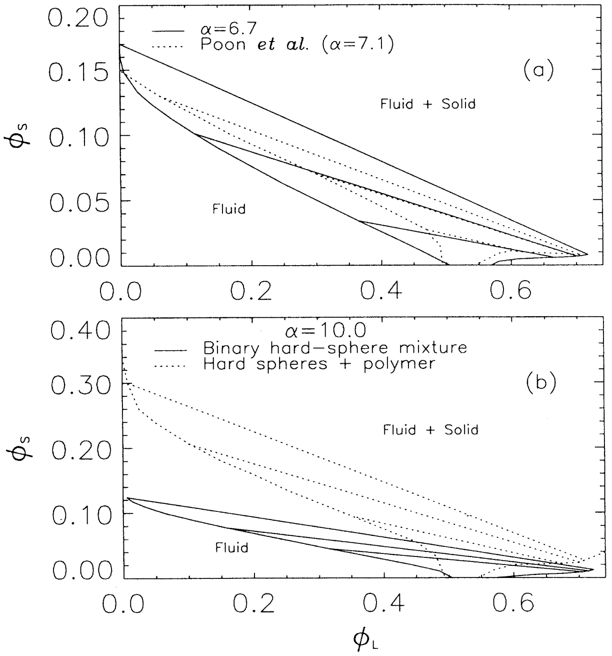

FIG. 6. (a) A phase diagram calculated from the present theory ($\alpha = 6.7$, solid curves) is compared to that of [10] ($\alpha = 7.1$, dotted curves). In (a) and (b), the curved lines represent liquidus curves while the straight lines are tie lines whose end points correspond to the volume fractions of the coexisting solid and fluid phases at equilibrium. (b) A phase diagram calculated from the present theory (for binary hard-sphere mixtures) is compared to that of Ref. [9] (for mixtures of hard spheres and polymer). The hard-core repulsion of the small particles dramatically widens the region of instability of the fluid phase.

Note added in proof. Phase separation in binary suspensions of silica spheres with $\alpha = 9.3$ was recently reported by A. Imhof and J. K. G. Dhont, Phys. Rev. Lett. **75**, 1662 (1995).

ACKNOWLEDGMENTS

We gratefully acknowledge illuminating discussions with L. E. Campbell, P. D. Kaplan, D. A. Boas, M. H. Kao, and T. C. Lubensky. We also thank Maria Zuckerman and Anthony Smith for their technical contributions. This work is supported by the National Science Foundation through Grant No. DMR93-06814 and through the Materials Research Laboratory Grant No. DMR91-20668. A.G.Y. also acknowledges partial support by the NSF through the PYI program and by the Alfred P. Sloan Foundation.

[1] For discussions on the application of thermodynamics and statistical mechanics to colloidal systems, see, for example, A. Vrij, Pure Appl. Chem. **48**, 471 (1976).

[2] See, for example, D. J. Pine, D. A. Weitz, J. X. Zhu, and E. Herbolzheimer, J. Phys. (Paris) **51**, 2101 (1990); A. G. Yodh, D. J. Pine, P. D. Kaplan, M. H. Kao, and N. Georgiades, Mol. Cryst. Liq. Sci. Technol. B Nonlinear Opt. **3**, 149 (1992).

[3] P. Pieranski, E. Dubois-Violette, F. Rothen, and L. Strzelecki, J. Phys. (Paris) **42**, 53 (1981).

[4] P. D. Kaplan, J. L. Rouke, A. G. Yodh, and D. J. Pine, Phys. Rev. Lett. **72**, 582 (1994).

[5] R. J. Buehler, R. H. Wentorf, Jr., J. O. Hirschfelder, and C. F. Curtiss, J. Chem. Phys. **19**, 61 (1951).

[6] W. G. Hoover and F. H. Ree, J. Chem. Phys. **49**, 3609 (1968); B. J. Alder, W. G. Hoover, and D. A. Young, *ibid.* **49**, 3688 (1968).

[7] See, for example, P. N. Pusey and W. van Megen, Nature (London) **320**, 340 (1986); S. E. Paulin and B. J. Ackerson, Phys. Rev. Lett. **64**, 2663 (1990).

[8] H. N. W. Lekkerkerker and A. Stroobants, Physica A **195**, 387 (1993).

[9] H. N. W. Lekkerkerker, W. C. K. Poon, P. N. Pusey, A. Stroobants, and P. B. Warren, Europhys. Lett. **20**, 559 (1992).

[10] W. C. K. Poon and P. B. Warren, Europhys. Lett. **28**, 513 (1994).

[11] S. Asakura and F. Oosawa, J. Chem. Phys. **22**, 1255 (1954).

[12] A. Vrij, Pure Appl. Chem. **48**, 471 (1976).

[13] J. L. Lebowitz and J. S. Rowlinson, J. Chem. Phys. **41**, 133 (1964).

[14] T. Biben and J. P. Hansen, Phys. Rev. Lett. **66**, 2215 (1991); J. Phys. Condens. Matter **3**, F65 (1991).

[15] Y. Rosenfeld, Phys. Rev. Lett. **72**, 3831 (1994).

[16] P. Bartlett and P. N. Pusey, Physica A **194**, 415 (1993); P. Bartlett, R. H. Ottewill, and P. N. Pusey, Phys. Rev. Lett. **68**, 3801 (1992); J. Chem. Phys. **93**, 1299 (1990); J. V. Sanders, Philos. Mag. A **42**, 705 (1980).

[17] A. R. Denton and N. W. Ashcroft, Phys. Rev. A **42**, 7312 (1990); M. D. Eldridge, P. A. Madden, and D. Frenkel, Mol. Phys. **79**, 105 (1993).

[18] P. Bartlett, J. Phys. Condens. Matter **2**, 4979 (1990).

[19] J. S. van Duijneveldt, A. W. Heinen, and H. N. W. Lekkerkerker, Europhys. Lett. **21**, 369 (1993).

[20] S. Sanyal, N. Easwar, S. Ramaswamy, and A. K. Sood, Europhys. Lett. **18**, 107 (1992).

[21] F. L. Calderon, J. Bibette, and J. Biais, Europhys. Lett. **23**, 653 (1993).

[22] H. De Hek and A. Vrij, J. Colloid Interface Sci. **84**, 409 (1981).

[23] S. M. Ilett, A. Orrock, W. C. K. Poon, and P. N. Pusey, Phys. Rev. E **51**, 1344 (1995).

[24] J. Bibette, D. Roux, and B. Pouligny, J. Phys. (France) II **2**, 401 (1992); J. Bibette, D. Roux, and F. Nallet, Phys. Rev. Lett. **65**, 2470 (1990).

[25] U. Steiner, A. Meller, and J. Stavans, Phys. Rev. Lett. **74**, 4750 (1995).

[26] A. P. Gast and W. B. Russel, J. Colloid Interface Sci. **106**, 251 (1983).

[27] See, for example, J. N. Israelachvili, *Intermolecular and Surface Forces with Applications to Colloidal and Biological Systems* (Academic, London, 1985); J. Gregory, Water Sci. Technol. **27**, 1 (1993).

[28] P. N. Pusey, A. D. Pirie, and W. C. K. Poon, Physica A **201**, 322 (1993).

[29] Random stacking of close-packed planes has been investigated in monodisperse hard-sphere colloids by P. N. Pusey, W. van Megen, P. Bartlett, B. J. Ackerson, J. G. Rarity, and S. M. Underwood, Phys. Rev. Lett. **63**, 2753 (1989).

[30] The attraction between large spheres and the wall has recently been investigated by P. D. Kaplan, L. P. Faucheux, and A. J. Libchaber, Phys. Rev. Lett. **73**, 2793 (1994).

[31] A. D. Dinsmore, L. E. Campbell, A. G. Yodh, and D. J. Pine (unpublished).

[32] N. F. Carnahan and K. E. Starling, J. Chem. Phys. **51**, 635 (1969).

[33] K. R. Hall, J. Chem. Phys. **57**, 2252 (1972).

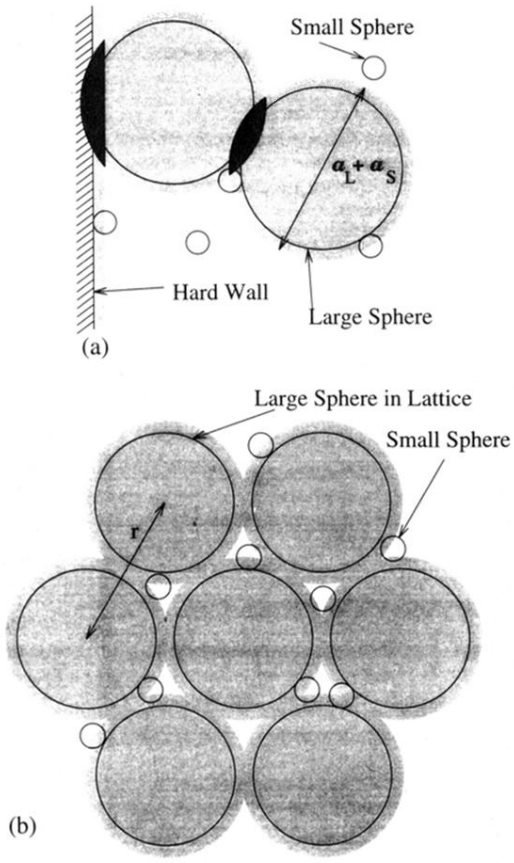

FIG. 1. Drawing of large and small spheres showing the excluded-volume regions described in the text. (a) The small-sphere centers of mass cannot penetrate within the shaded regions. When the large spheres approach one another or the wall, these excluded-volume regions overlap, increasing the volume accessible to the small spheres by the volume of the heavily shaded regions. (b) Diagram of the solid phase. The white regions represent the volume accessible to the small spheres, defined in Sec. IV as $(\xi + \gamma)V$.

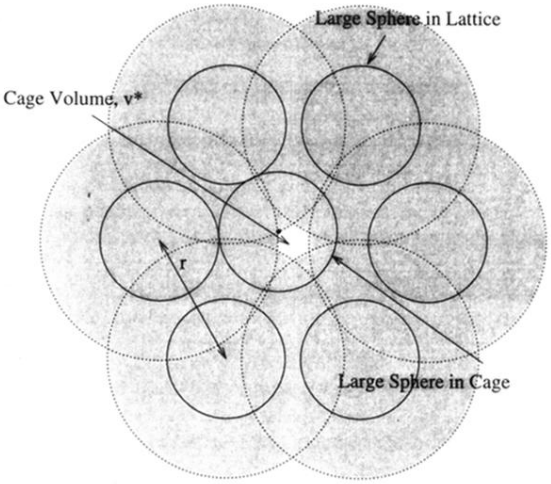

FIG. 4. Diagram of the large-sphere crystal. Due to the hard-core repulsion, the middle sphere's center of mass can fit only in the small central white region which is a two-dimensional slice of the cage volume, v^*.